

High Harmonic ECH Experiment for Extension of Heating Parameter Regime in LHD^{*})

Takashi SHIMOZUMA, Hiromi TAKAHASHI, Shin KUBO, Yasuo YOSHIMURA, Hiroe IGAMI, Masaki NISHIURA, Shinya OGASAWARA, Ryohei MAKINO, Hiroshi IDEI¹⁾, Nikolai B MARUSHCHENKO²⁾, Yuri TURKIN²⁾ and Takashi MUTOH

National Institute for Fusion Science, 322-6 Oroshi-cho, Toki 509-5292, Japan

¹⁾*Research Institute for Applied Mechanics, Kyushu University, 6-1 Kasuga-koen, Kasuga, Fukuoka 816-8580, Japan*

²⁾*Max-Planck-Institut für Plasmaphysik, EURATOM-Association, Greifswald, Germany*

(Received 7 December 2012 / Accepted 1 April 2013)

High harmonic electron cyclotron resonance heating (ECH) can extend the plasma heating region to higher density and higher β compared to the normal heating scenario. In this study, the heating characteristics of the second-harmonic ordinary (O2) and third-harmonic extraordinary (X3) modes and the possible extension of heating regime are experimentally confirmed. At the same time, a comparative study using ray-tracing calculation was performed in the realistic three-dimensional configuration of the Large Helical Device. The O2 mode heating showed a 40% absorption rate even above the X2 mode cut-off density. The X3 mode heating using powerful 77 GHz gyrotrons demonstrated an increase of about 40% in the central electron temperature in the plasmas at β -value of about 1%. These results were quantitatively explained to some extent by ray-tracing calculations.

© 2013 The Japan Society of Plasma Science and Nuclear Fusion Research

Keywords: electron cyclotron heating, ECH, high harmonic heating, gyrotron, absorption rate, ray-tracing, LHD

DOI: 10.1585/pfr.8.2402073

1. Introduction

High harmonic electron cyclotron heating (ECH) is an effective method of extending the operational regime to high density and high β by alleviating the density limitation due to some cut-offs of EC wave propagation even in a low magnetic field [1–4]. Instead of the normally used fundamental ordinary (O1) mode and the second-harmonic extraordinary (X2) mode heating procedures, an adequate absorption rate will be expected using the second-harmonic ordinary (O2) mode and the third-harmonic extraordinary (X3) mode heating scenarios, when the temperature and density of a target plasma are sufficiently high [5]. For example, the cut-off densities of X3 and O2 mode wave propagation are 4/3 times and twice the X2 mode cut-off density, respectively. The objective of this research is to confirm the effectiveness of the X3 and O2 mode heating scenarios experimentally in the Large Helical Device (LHD).

In LHD, two frequencies, i.e., 77 GHz and 154 GHz are being used for ECH. For these frequencies, Fig. 1 indicates the extent of the plasma density to be heated for each heating mode and EC resonant magnetic field strength. The normally used heating scenarios, O1 and X2, are indicated by red arrows in Fig. 1, and good absorption is expected for these modes. At low magnetic fields (below 1.375 T), O2 and X3 mode heating using 77 GHz gy-

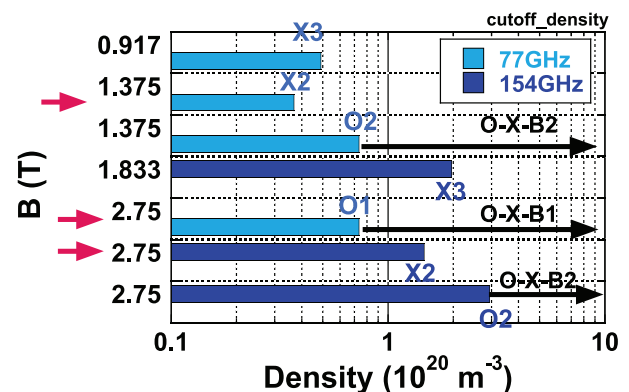


Fig. 1 Relation between heating mode and possible hearing extent using 77 and 154 GHz gyrotrons in LHD.

rotrons can extend the heating region to the higher density and higher β area. Furthermore, at higher magnetic fields (around 1.833 and 2.75 T), the cut-off densities for X3 and O2 mode propagation using 154 GHz reach the fusion-relevant densities, $2.2 \times 10^{20} \text{ m}^{-3}$ and $3 \times 10^{20} \text{ m}^{-3}$, respectively.

2. ECH System in LHD and Achieved Injection Power

To increase the ECH power injected into LHD, we have been developing and installing 77 and 154 GHz

author's e-mail: shimozuma.takashi@LHD.nifs.ac.jp

^{*}) This article is based on the presentation at the 22nd International Toki Conference (ITC22).

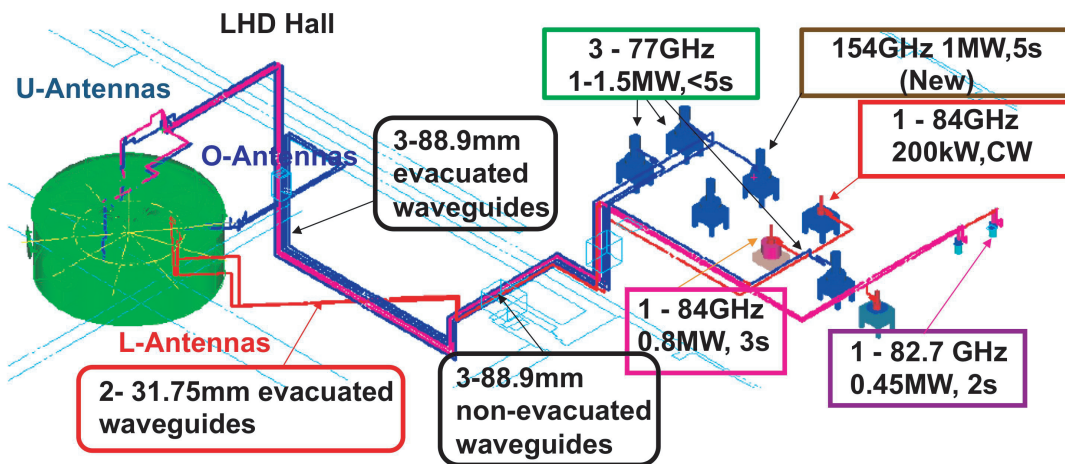


Fig. 2 Present (2012) ECH system in LHD.

Table 1 Achieved parameters of the developed gyrotrons: three 77 GHz gyrotrons and one 154 GHz gyrotron.

Tube No.	Specification	Pulse Operation <5 s	CW Operation
#1 R	1 MW/ 5 s 0.3 MW/ CW	1.01 MW (33.0 %) 5 s	0.29 MW (29.2 %) 60 s 0.13 MW (21.7 %) 935 s
	Two step V_A rise	1.41 MW (51.1 %) 0.2 s	
#2 (R)	1.2 MW/ 5 s 0.3 MW/ CW	1.02 MW (30.3 %) 5 s	0.2 MW (19.8 %) 370 s *0.24 MW (30.8%) 1800 s *0.3 MW (31.3 %) 165 s
	Two step V_A rise	1.30 MW (43.8 %) 0.45 s	
#3	1.5 MW/ 2 s 1.2 MW/ 10 s 0.3 MW/ CW	1.53 MW (36.0 %) 1.6 s	0.30 MW (36.3 %) 2400 s 0.22 MW (32.4%) 4500 s
	Two step V_A rise	1.87 MW (37.2 %) 0.1 s 1.78 MW (37.9 %) 1 s	
#4 (154GHz)	1 MW/ 5s 0.5 MW/ CW	1.16 MW (36.9 %) 1 s	-

Output power (Efficiency) Pulse width

gyrotrons under collaboration with the University of Tsukuba. A schematic view of the present ECH system in LHD is shown in Fig. 2. The ECH system is composed of seven gyrotron systems. There are three 77 GHz gyrotrons and one 154 GHz gyrotron with more than 1 MW of output power. The other gyrotrons operate at 84 GHz with 0.2 MW/CW, 84 GHz with 0.8 MW/3 s and 82.7 GHz with 0.45 MW/2 s.

Three types of antenna are used. One is a top-launching antenna composed of four mirrors at the upper port of LHD, which is called the U-port antenna. The other is a lateral injection one consisting of two mirrors at the lateral outer port of LHD, the so called O-port antenna. The third type of antenna is a bottom-launching one at a lower port. The final mirror of each antenna can be steered to

change the focal position in the plasma. The millimeter-wave power is transmitted through evacuated corrugated waveguides 88.9 mm or 31.75 mm in diameter as shown in Fig. 2.

The 77 and 154 GHz gyrotrons with more than 1 MW of power have been developed in cooperation with the University of Tsukuba since 2006. The performance of the gyrotrons, such as their output power and available pulse width, has been improved step by step. The achieved parameters of each gyrotron are summarized in Table 1. A 154 GHz gyrotron was just installed in 2012 and is being tested in the LHD ECH system. It has already delivered more than 1 MW with 1 second pulse width into LHD.

3. Experimental Results and Comparison with Ray-Tracing Calculations

3.1 Second-harmonic ordinary (O2) mode heating above plasma cut-off density

A target plasma was sustained by neutral beam injection (NBI) power, and its density was ramped up from $2 \times 10^{19} \text{ m}^{-3}$ to $6 \times 10^{19} \text{ m}^{-3}$ above the X2 cut-off density ($3.7 \times 10^{19} \text{ m}^{-3}$) in a discharge time of 2 s. O- and X- mode polarized waves were injected from the O-port antenna, which was installed in the horizontally elongated plasma cross section. In this configuration, the wave could be injected almost perpendicularly to the electron cyclotron resonance (ECR) layer, and the inflection effect of the wave was expected to be small. The magnetic strength at the magnetic axis of 3.6 m was 1.43 T. Five ECH pulses with pulse width 200 ms and power 1 MW were injected every 300 ms. During the shot, the central electron temperature decreased from 1.5 to 1 keV with the electron density increase. The absorption rate of the O2 and X2 mode power for each pulse could be estimated by calculating the increment dW_p/dt just before and after the turn-on and turn-off timing of each ECH pulse. The density dependence of the absorption rate is plotted in Fig. 3.

The vertical dashed line corresponds to the cut-off density of the X2 mode ($3.7 \times 10^{19} \text{ m}^{-3}$). For this mode, the maximum absorption rate reaches 80%, whereas it is 50% for the O2 mode. Above the cut-off density of the X2 mode, however, the absorption rate of the O2 mode exceeds that of the X2 mode. This indicates effective heating of the O2 mode above the cut-off density of the X2 mode. Non-absorbed RF signals detected by a sniffer probe [6, 7], which is installed in the same port as the antenna, show a continuous increase over the cut-off density for X2 mode injection. In contrast, the non-absorbed electro-magnetic wave signal for O2 mode injection does not change very much over a wide density range. The behavior of the snif-

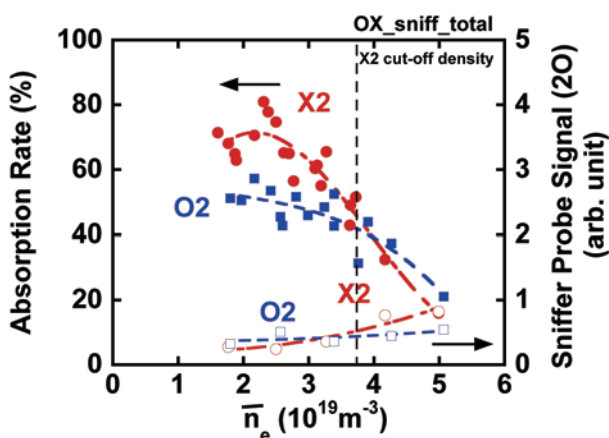


Fig. 3 Dependence of absorption rate and scattered power on line-averaged density. The scattered RF power was detected by a sniffer-probe.

fer probe signals indicates that O2 mode absorption is not affected by the X2 cut-off density, although its absorption is determined mainly by the low electron temperature.

Ray-tracing calculations using the TRAVIS code [8] were also performed for the same magnetic and injection conditions. In Fig. 4(a), the results show 100% absorption of the X2 mode below the X2 mode cut-off density and a sharp decrease in the absorption to zero just above the cut-off. In contrast, the absorption of the O2 mode increases gradually with the density and reaches a maximum of about 40% around $4.5 \times 10^{19} \text{ m}^{-3}$. Figure 4(b) clearly indicates the effective absorption between the two resonances in the lateral injection case.

These behaviors agree qualitatively with the experimental results. However, the variation in the electron temperature with the density and a multi-reflection effect should be considered to explain the difference in the absolute values of the absorption.

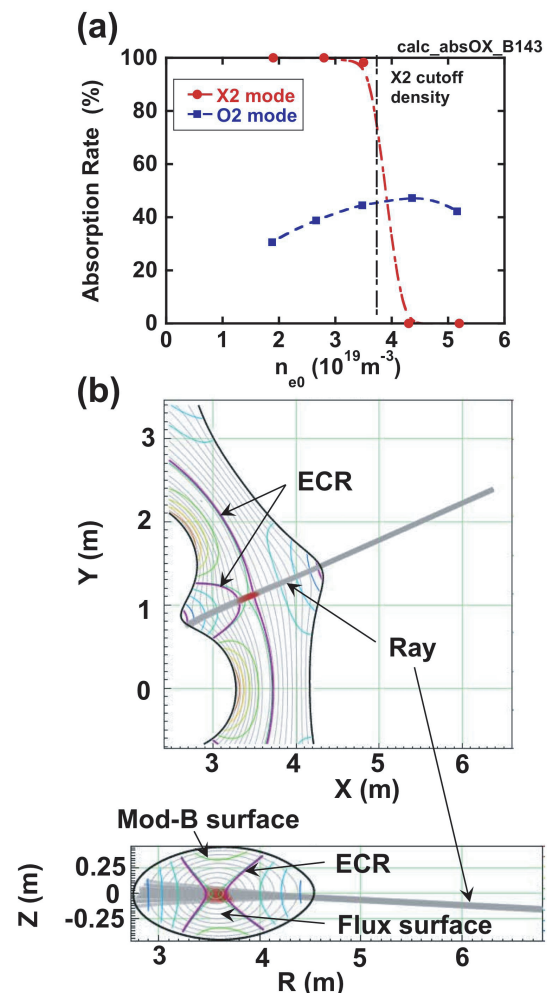


Fig. 4 Ray-trace calculation of O2 heating (a) Absorption rate vs. central electron density, (b) example of calculated rays and absorbed area on toroidal and poloidal planes. Red indicates wave absorption areas.

3.2 Optimization of third harmonic extraordinary (X3) mode heating

For ECH power injection from the U-port antenna in a vertically elongated plasma cross-section, the heating position and efficiency depend strongly on the focal position of the beam. For X3 mode heating, the dependence of the absorption rate on the focal position of the U-antenna injection was investigated. A target plasma was sustained by NBI; its electron density, temperature and β -value were $0.7 \times 10^{19} \text{ m}^{-3}$, about 1.2 keV and 0.6%, respectively. The absorption rate was evaluated at the on- and off-timing of the ECH pulses. Figure 5 (a) shows the absorption rate, P_{abs}/P_0 , as a function of the radial focal position on the equatorial plane R_f of the U-port antenna (9.5U port). The third-harmonic ECR exists at $R = 3.74 \text{ m}$. The absorption rate has maxima around $R_f \sim 3.64 \text{ m}$ for on-timing estimation and around $R_f \sim 3.7 \text{ m}$ for off-timing estimation, although the data points are slightly scattered. The time variations in the non-absorbed electro-magnetic wave signals that were detected by a sniffer probe installed at the lower port (9.5L port) just opposite the U-port antenna are

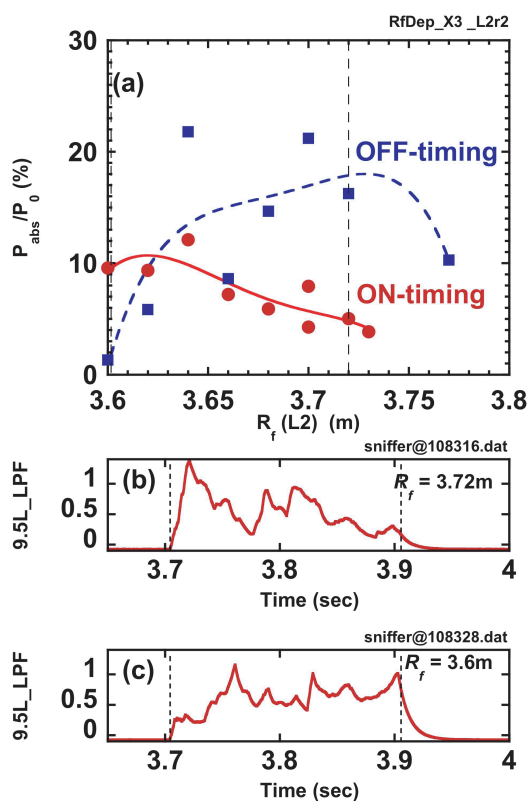


Fig. 5 (a) Absorption rate for U-port antenna (9.5U) as a function of radial focal position R_f (m). The values were evaluated at the on- (closed circles) and off-timing (closed squares) of the ECH pulse. (b) Time variation in low-pass-filtered sniffer probe signal detected at L-port for $R_f = 3.72 \text{ m}$. (c) Time variation in sniffer probe signal for $R_f = 3.6 \text{ m}$. ECH was on between dashed vertical lines in (b) and (c).

also plotted in Fig. 5 (b) and 5 (c) for $R_f \sim 3.72 \text{ m}$ and for $R_f \sim 3.6 \text{ m}$, respectively. The signals were time-averaged by a low-pass-filter. For $R_f = 3.72 \text{ m}$ shown in Fig. 5 (b), the sniffer probe signal exhibits a decreasing trend during the ECH pulse, indicating that wave absorption improved toward the end of the pulse. On the other hand, for $R_f = 3.6 \text{ m}$ shown in Fig. 5 (c), the sniffer probe signal gradually increased, suggesting that wave absorption deteriorates toward the end of the pulse. The sniffer probe signal levels around the ECH on- and off-timings can partly explain the difference in the absorption rate evaluated at the on- and off-timings for $R_f = 3.6 \text{ m}$ and $R_f = 3.72 \text{ m}$ indicated by the vertical dashed lines shown in Fig. 5 (a). This suggests that changes in the temperature and density at the focal point strongly affect the wave trajectory and absorption. The experimental results yield the information on the optimum antenna setting for the best absorption.

A change in the hitting position on the graphite target plate installed in the 9.5L-port opposed the U-port antenna with and without plasma clearly shows a deflection of the wave beam by the plasma and the necessity of feedback control of the antenna focal point according to changes in the plasma parameters.

Figure 6 shows the electron temperature and density profiles before and during stair-like ECH power injection. Using three 77 GHz gyrotrons, a total of 2.9 MW of power was injected during the highest-power injection period. The central electron temperature increased significantly by about 40% with almost constant density.

Ray-tracing analyses were performed for the same plasma parameters as in the experiment. In Fig. 7, the focal position dependences of the absorption rate are plotted for injection from the U-port antenna in (a) and from the O-port antenna in (c). The typical ray trajectories are shown in (b) for U-port injection and in (d) for O-port injection. The focal position yielding the peak absorption differs slightly between the experimental and ray-tracing results shown in Figs. 5 (a) and 7 (a). In addition, a dis-

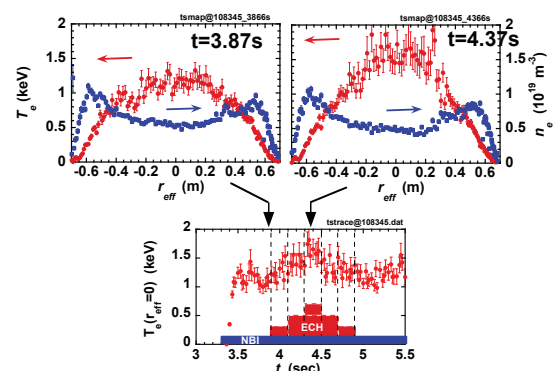


Fig. 6 Electron temperature and density profiles during high-power X3 ECH. Time trace of central electron temperature is also plotted.

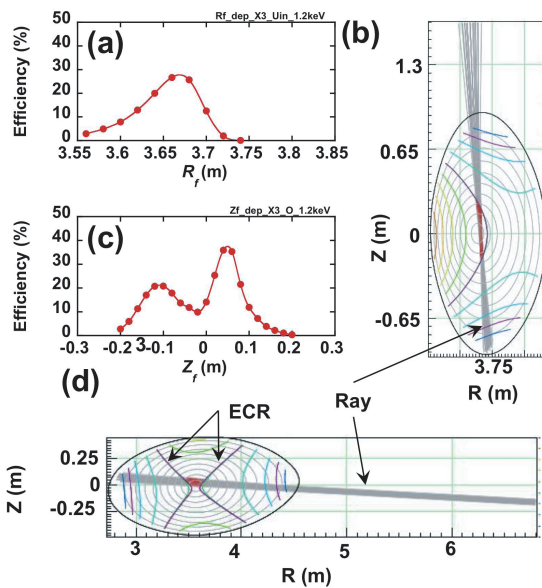


Fig. 7 Ray-trace calculation of X3 mode heating, (a) Focal position dependence of absorption rate and (b) rays for U-port injection ($R_f = 3.65$ m). (c) Focal position dependence of absorption rate and (d) rays for O-port injection ($Z_f = 0$).

crepancy in the value of the absorption rate also exists. The calculated ray trajectories shown in Fig. 7 (b) correspond to the ray trajectories that achieved the maximum absorption rate ($R_f = 3.66$ m). The rays cross the ECR line twice and pass through the slightly higher-field side of the ECR line on the equatorial plane. Figure 7 (c) shows a double peak in the Z_f dependence. This result implies that there is an optimum distance between the two ECR layers that yields the maximum absorption rate, as shown in Fig. 7 (d).

4. Summary

The heating characteristics of high harmonic ECH, in particular second ordinary (O2) and third extraordinary (X3) mode heating, were experimentally investigated to confirm the effectiveness of heating in higher-density and higher- β plasmas. In O2 mode heating of plasmas above the X2 mode cut-off density ($3.7 \times 10^{19} \text{ m}^{-3}$), the absorption rate of the O2 mode exceeded that of the X2 mode, showing an extension to a higher-density region. In the X3 mode heating experiment, an optimized antenna fo-

cal position from the U-port antenna could be obtained. The optimal focal positions were observed to shift during the ECH pulse. Deflection of the wave beam was experimentally observed using a target plate installed opposite the antenna. A maximum central temperature rise of about 40% was attained by 2.9 MW injection into a plasma with $T_{e0} \sim 1.2$ keV and a line-averaged electron density of $\sim 0.7 \times 10^{19} \text{ m}^{-3}$. Ray-tracing calculations using the TRAVIS code were conducted and compared with the experimental data.

Acknowledgement

The authors gratefully acknowledge the LHD experiment group for their operation of LHD, and the heating and diagnostic devices. They also thank Doctors R. Minami, T. Kariya and T. Imai at the University of Tsukuba for the development of the powerful gyrotrons. This work was supported by NIFS under ULRR701, 801, and 804. This work was also supported by a Grant-in-Aid for Scientific Research from the Ministry of Education, Science and Culture of Japan (24560066).

- [1] U. Gasparino, H. Idei, S. Kubo, N. Marushchenko and M. Romé, Nucl. Fusion **38**, 223 (1998).
- [2] T. Shimozuma, H. Idei, S. Kubo, T. Takita, S. Kobayashi, S. Ito, Y. Mizuno, M. Sato, K. Ohkubo, Y. Yoshimura *et al.*, 27th European Physical Society Conference on Controlled Fusion and Plasma Physics, Budapest, Hungary, June 12-16, 2000, P4.019.
- [3] S. Alberti, T. P. Goodman, M.A. Henderson, A. Manini, J.-M. Moret, P. Gomez, P. Blanchard, S. Coda, O. Sauter, Y. Peysson and TCV Team, Nucl. Fusion **42**, 42 (2002).
- [4] S. Alberti, G. Arnoux, L. Porte, J.-P. Hogge, B. Marletaz, P. Marmillod, Y. Martin, S. Nowak and TCV Team, Nucl. Fusion **45**, 1224 (2005).
- [5] T. Shimozuma, S. Kubo, H. Igami, Y. Yoshimura, T. Notake, N.B. Marushchenko, Y. Turkin, T. Mutoh and LHD Experiment Group, Plasma Fusion Res. **3**, S1080 (2008).
- [6] H. Igami, S. Kubo, H.P. Laqua, K. Nagasaki, S. Inagaki, T. Notake, T. Shimozuma, Y. Yoshimura, T. Mutoh and LHD Experiment Group, Rev. Sci. Instrum. **77**, 10E931 (2006).
- [7] F. Gandini, S. Cirant, M. Hirsch, H.P. Laqua, S. Nowak, A. Bruschi, G. Granucci, V. Erckmann, V. Meller, V. Muzzini, A. Nardone, A. Simonetto, C. Sozzi and N. Spinichia, Fusion Eng. Des. **56-57**, 975 (2001).
- [8] N.B. Marushchenko, V. Erckmann, H.J. Hartfuss, M. Hirsch, H.P. Laqua, H. Maassberg and Y. Turkin, Plasma Fusion Res. **2**, S1129 (2007).